Hybrid Electric Propulsion Using Doubly-Fed Induction Machines

Marc Bodson[1]
University of Utah, Salt Lake City, Utah, 84112

David J. Sadey[2], Keith R. Hunker[3], Casey J. Theman[4], Linda M. Taylor[5] and Jeffrey T. Csank[6]
NASA Glenn Research Center, Cleveland, OH, 44135

The paper considers a hybrid electric propulsion architecture where most of the electric power is transmitted from the generator to the motors without conversion. Doubly-fed induction machines are chosen for generation and propulsion, due to their ability to operate over a range of speeds using reduced-size power converters. The focus of the paper is on the presentation and demonstration of a strategy that allows for the stable and independent operation of multiple motors using the power produced by a single generator. The control methodology includes synchronization, soft-start, and closed-loop speed control of each motor as a means of controlling output thrust. The validation is carried out on a low power test bed using fractional horsepower machines. The success obtained at a small scale suggests that the proposed strategy would be worth evaluating at higher power levels, with a potential application to commercial transport aircraft.

Nomenclature

AC	Alternating Current
CB	Contactor Breaker
COTS	Commercial Off-The-Shelf
CT	Current Transducer
DC	Direct Current
DFIM	Doubly-Fed Induction Machine
DFI Motor	Doubly-Fed Induction Motor
DFIG	Doubly-Fed Induction Generator
LPTB	Low Power Test Bed
PF	Power Factor
PMDC	Permanent-Magnet DC
PT	Potential Transducer
RSC	Rotor Side Converter
a,s , b,s , c,s	Subscripts for phases a,b,c of the stator
a,r , b,r , c,r	Subscripts for phases a,b,c of the rotor
$C_m(s)$	Compensator for the grid magnitude
$C_p(s)$	Compensator for the grid phase
f_{ref}	Stator reference frequency, Hz
Im	Imaginary part of a complex number
I_r	Rotor current phasor, A
I_s	Stator current phasor, A
L_r	Rotor inductance, H
L_s	Stator inductance, H
M	Stator/rotor mutual inductance, H
n_p	Number of pole pairs
P_m	Mechanical power, W
P_r	Rotor electrical power, W
P_s	Stator electrical power, W
Q_{com}	Reactive power command, VAR
Q_r	Rotor reactive power, VAR
Q_s	Stator reactive power, VAR
Re	Real part of a complex number
R_r	Rotor resistance, Ω
R_s	Stator resistance, Ω
s_n	Normalized slip (per-unit)
v_g	Grid voltage vector, V
$v_{r,com}$	Rotor voltage magnitude command, V
$v_{m,s}$	Stator voltage magnitude, V
v_r	Rotor voltage vector, V
V_r	Rotor voltage phasor, V
v_{ref}	Stator voltage magnitude reference, V
v_s	Stator voltage vector, V

[1] Professor, Electrical and Computer Engineering, bodson@eng.utah.edu, AIAA Associate Fellow.
[2] AST, Power Management and Distribution Branch, david.j.sadey@nasa.gov.
[3] AST, Diagnostics & Electromagnetics Branch, keith.r.hunker@nasa.gov.
[4] AST, Space Power and Propulsion Test Engineering Branch, casey.j.theman@nasa.gov.
[5] AST, Power Management and Distribution Branch, linda.m.taylor@nasa.gov.
[6] AST, Power Management and Distribution Branch, jeffrey.t.csank@nasa.gov, AIAA Sr. Member.

V_s	Stator voltage phasor, V	τ_m	Torque, N.m
$\delta\theta_r$	Rotor angle error variable, rad	ω_m	Rotor speed, rad/s
θ_c	Feedforward angle correction, rad	ω_r	Rotor electrical angular frequency, rad/s
θ_m	Rotor angle of the motor, rad		
θ_{ref}	Grid voltage angle reference, rad	ω_{ref}	Motor speed reference, rad/s
$\theta_{r,com}$	Rotor voltage angle command, rad	ω_s	Stator electrical angular frequency, rad/s
θ_s	Stator electrical angle, rad		
τ_{com}	Torque command, N.m		

I. Introduction

HYBRID electric propulsion provides opportunities to build large transport aircraft with less noise, higher fuel and energy efficiency, and reduced emissions [1]. Synergistic design and integration of the power system into the airframe may be needed to provide the full benefits of such technology [2]. For example, the integration of a liquid hydrogen fueled hybrid-electric distributed propulsion system with the airframe of an Ultra High Capacity Blended Wing Body configuration is explored in ref. [3]. Further synergy may involve distributed propulsion [4] as well as flexible wings [5] to reduce fuel burn by exploiting multidisciplinary interactions. At a smaller scale, ref. [6] analyzes the potential for improvement in energy efficiency and mission flexibility in the context of commercial skydiving missions (short flights between 15 and 20 min to a height of 4000 m). Ref. [7] considers the design and sizing process of a hybrid-electric propulsion system for a single-seat demonstrator aircraft and ref. [8] reviews existing and current developments of hybrid-electric propulsion systems for small fixed-wing Unmanned Aerial Vehicles. With a different focus, ref. [9] discusses a terminal area operations analysis software that anticipates the nuances of hybrid electric distributed propulsion, including unique failure modes and powered-lift effects.

The most common architecture of hybrid electric propulsion is shown in Fig. 1. The approach relies on two power conversion stages to transmit the power extracted off the turbine-driven generator to the motor driving the propulsor fan. The power must be converted from alternating current (AC) to direct current (DC) and then back to AC, requiring two full power rated converters. The architecture is referred to as *hybrid electric* if storage is included as shown on Fig. 1, and *turbo-electric* otherwise.

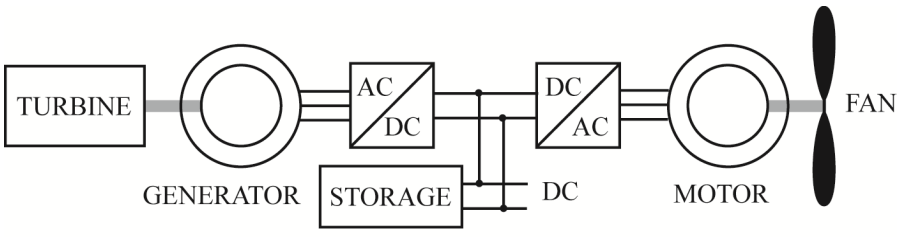

Fig. 1. DC power architecture

Power electronic converters contribute significantly to the overall weight and efficiency of the system, so methods to reduce their impact are of great benefit. Towards that goal, a primarily AC system was proposed in ref. [10]. The concept uses doubly-fed induction machines (DFIMs), as shown in Fig. 2. In this system, the majority of the power can be transferred from the generator to the motor without conversion. The remaining, fractional power, is processed through smaller power electronic converters feeding the rotors of the machines. A relatively small energy storage element is included on the figure that assists in the operation. A strong motivating factor for the consideration of DFIMs in electric propulsion is that a large fraction of wind power installations worldwide use doubly-fed induction generators, so there is evidence that these machines are advantageous at the power levels under consideration and with competitive efficiencies, while permitting operation at variable speeds.

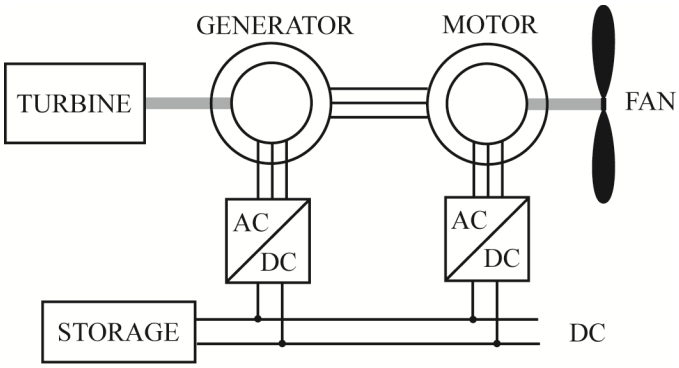

Fig. 2. DFIM-based AC power architecture

A hybrid electric propulsion system may also involve multiple motors connected in parallel on a single AC supply provided by the generator, with each motor being controlled by its own reduced-size converter. In this case, the architecture is referred to as *distributed electric propulsion* (DEP). With DFIMs used for generation and propulsion, it is theoretically possible to control the speeds of the motors independently of each other, and independently of the frequency of the stator voltages. It is also possible for the generator to produce a voltage with a frequency independent of the turbine speed. Nevertheless, these variables should be optimized for efficiency and performance, while ensuring that device constraints are satisfied.

The main question addressed in this paper is whether this proposed architecture is viable in practice. Would instabilities develop in such a system that could cause, for example, a voltage collapse on the AC link? Would multiple motors interact in negative ways so that the performance or safety of the system would be compromised? The evidence presented in the paper shows not only that stable control of the generator and of three motors can be achieved, but also

that the result can be obtained with relatively simple control strategies. Each motor can be smoothly connected to the generator's three-phase stator at standstill, and then made to follow specified speed profiles. Experimental results obtained on a low power test bed demonstrate a very good performance of the system, including with profiles that emulate flight from take-off to landing and include equal as well as differential speed commands to the motors. However, the design of a higher level of control ensuring optimal operation and storage management, together with the protection of the devices, is left as a subject of future research.

A preliminary paper [11] presented results for the case where the AC voltages were supplied by a power supply with fixed frequency and voltage. The results of this paper show that similar results are obtained when the supply is a generator whose voltages change deliberately or under load. Variations of the speed of the generator and of the generated frequency are also applied, with a high level of decoupling achieved.

The conclusions to be drawn from the study are limited by the low power level of the hardware that was used in the tests. Nevertheless, the validation provides support for experimentation at larger power levels, and optimism regarding the use of the proposed solution for hybrid electric propulsion in future transport aircraft.

The paper proceeds as follows. First, a review of DFIMs is presented together with the control strategy used for the motors and generator (Section II). Then, the hardware and the test results are described (Section III). The relative advantages of different architectures, including the proposed one, are discussed (Section IV) and topics of future research are described (Section V). Finally, the paper ends with some concluding remarks (Section VI).

II. Doubly-Fed Induction Machines and Their Control

A. Doubly-Fed Induction Machines

Doubly-fed induction machines can be used as motors or generators. In addition to the abbreviation DFIM, we will use the abbreviations DFI motor for doubly-fed induction motor and DFIG for doubly-fed induction generator. The DFIM (also called a *wound-rotor induction machine*) has historically received limited use as an induction motor with variable rotor resistance, which was obtained by connecting the rotor windings to stationary, variable resistors. Developments in power electronics have made new modes of operation possible. The DFIM has been used especially as a variable-speed generator in wind turbine applications [12]. The advantage of the DFIM as a generator is that it can be designed and exploited in such a way that the power electronics required to control the generator are relegated to the rotor windings, with a reduction of the size of the power converter.

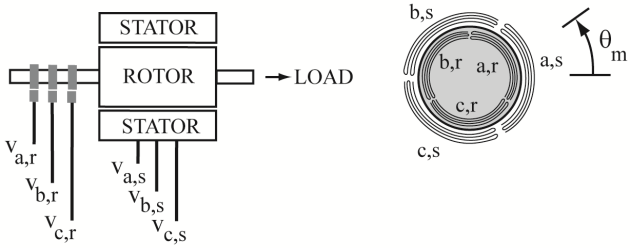

Fig. 3. DFIM structure

Fig. 3 shows the structure of a DFIM. On the left is a side view of the machine and on the right is a front view (*i.e.*, from the shaft) showing three-phase stator windings and three-phase rotor windings (in a simplified representation). The line-neutral voltages applied to the stator windings are labelled $v_{a,s}$, $v_{b,s}$, and $v_{c,s}$, while the line-neutral voltages applied to the rotor are labelled $v_{a,r}$, $v_{b,r}$, and $v_{c,r}$. The rotor voltages are applied through slip rings, as shown to the left of Fig. 3. The angle of the rotor winding *a,r* with respect to the stator winding *a,s* defines the rotor angular position, denoted θ_m. The angular velocity is denoted $\omega_m = d\theta_m/dt$. The shaft is connected to the load, in the case of a motor, or a prime mover in the case of a generator.

In steady-state, the stator voltages are sinusoidal variables with angular frequency ω_s, and can be represented by a single complex variable V_s (typically called a *phasor*) such that:

$$v_{a,s} = \mathrm{Re}\left(V_s\, e^{j\theta_s}\right), \tag{1}$$

$$v_{b,s} = \mathrm{Re}\left(V_s\, e^{j\theta_s - j2\pi/3}\right), \tag{2}$$

$$v_{c,s} = \mathrm{Re}\left(V_s\, e^{j\theta_s + j2\pi/3}\right), \tag{3}$$

where $\theta_s = \omega_s t$. The total active (P_S) and reactive (Q_S) powers absorbed by the stator windings are given by:

$$P_s + jQ_s = \frac{3}{2} V_s I_s^* \ , \tag{4}$$

where I_S^* is the complex conjugate of the phasor for the stator current.

The rotor voltages are sinusoidal variables described by phasors similarly to (1)-(3), but with phasor V_r and angle $\theta_r = \theta_s - n_p\theta_m$, where n_P is the number of pole pairs of the machine (n_P is equal to 1 on Fig. 3). The angular electrical frequency of the rotor voltages is:

$$\omega_r = \frac{d\theta r}{dt} = \omega_s - n_p \omega_m. \tag{5}$$

One defines s_n, the *normalized or per-unit slip*, as:

$$s_n = \frac{\omega_r}{\omega_s}. \tag{6}$$

Note that the rotor electrical frequency, ω_r, and the slip can be negative, which corresponds to an angle θ_r for the rotor voltage rotating in the counter-clockwise direction, *i.e.,* three-phase rotor voltages in reverse or backward sequence. Defining a rotor current phasor I_r, the total active and reactive powers absorbed by the rotor are defined as for the stator (4).

With these definitions, and assuming that the stator and rotor windings are connected in *Y* or Δ, the DFIM can be described by the following equations:

$$V_s = R_s I_s + j\omega_s (L_s I_s + M I_r), \tag{7}$$

$$V_r = R_r I_r + j\omega_r (L_r I_r + M I_s), \tag{8}$$

$$\tau_m = \frac{3}{2} n_p M \, \mathrm{Im}(I_s I_r^*). \tag{9}$$

In these equations, R_s is the resistance of the stator windings, R_r is the resistance of the rotor windings, L_s is the inductance of the stator windings, L_r is the inductance of the rotor windings, M is the mutual inductance between stator and rotor windings, τ_m is the torque and "Im" refers to taking the imaginary part of a complex number. The electrical parameters are equivalent line-neutral values in a *Y* configuration, and the torque is defined positive if motoring with $\omega_m > 0$.

Neglecting losses in the machine, the mechanical power produced by the machine (P_m, where P_m is positive if motoring with $\omega_m > 0$) is the sum of the electrical power supplied to the stator and rotor windings:

$$P_m = \tau_m \, \omega_m = P_s + P_r. \tag{10}$$

It turns out that the distribution of power between stator and rotor is solely determined by the relative speed of the motor compared to the frequency of the stator variables. Specifically, still neglecting losses and with $\omega_m > 0$, (7)-(10) yield:

$$P_s = \frac{\omega_s}{n_p \omega_m} P_m \tag{11}$$

$$P_r = -\frac{\omega_r}{\omega_s} P_s = -\frac{\omega_r}{n_p \omega_m} P_m. \tag{12}$$

An interesting property of the DFIM is that it can operate in sub- or super-synchronous modes relative to the frequency ω_s. Consider the case of a motor. For positive torque and speed, $P_s > 0$ and one has $P_r > 0$ for $n_p \omega_m > \omega_s$ (the super-synchronous case with $s_n<0$) while $P_r < 0$ for $n_p \omega_m < \omega_s$ (the sub-synchronous case with $s_n>0$). The super-synchronous case is particularly interesting because power is absorbed by the stator and the rotor to produce mechanical power. For operation as a DFIG, the super-synchronous case corresponds to power being generated by the stator and rotor windings.

For both motor and generator modes, the power converted on the rotor windings is smaller than the power converted on the stator windings for normalized slip smaller than one, and much smaller if the slip is a small fraction of unity. In any case, the power relationship (12) highlights the dual roles of the rotor, enabling the control of the torque and a stable operation, while also providing an additional path for conversion of electrical energy to mechanical energy.

B. DFI Motor Control

Concepts for the control of doubly-fed induction motors can be found in refs. [13]-[15]. There is also significant work on the two-converter operation of DFI motors [16]-[19], but this is a different design choice than the single converter structure adopted here, which loses its benefits in terms of converter power. Advanced algorithms for sensorless control (*i.e.,* without position sensors) are found in ref. [20]. The algorithm used for this project is different from the conventional approaches that use an inner current control loop along with an outer speed control loop. Instead, the speed is regulated using a single control loop, which is simpler and easier to tune. Nevertheless, versions with and without a current control loop are available in ref. [22].

The basis of the method is the steady-state model of the machine (7)-(9), as opposed to the full differential equation model. The experimental section in this paper shows that the tracking performance is accurate and responsive for the application under consideration, despite a relatively simple algorithm. Fig. 4 shows a block diagram of the control algorithm used for the DFI motor. The stator windings are connected to a three-phase supply (labelled grid) through a relay. In early experiments [11], the grid was obtained from an AC three-phase power supply. In this paper, the grid

is provided by a DFIG, constituting a weaker grid. Ultimately, three motors are connected in parallel on the grid, so that three identical copies of the algorithm of Fig. 4 are coded in the control software.

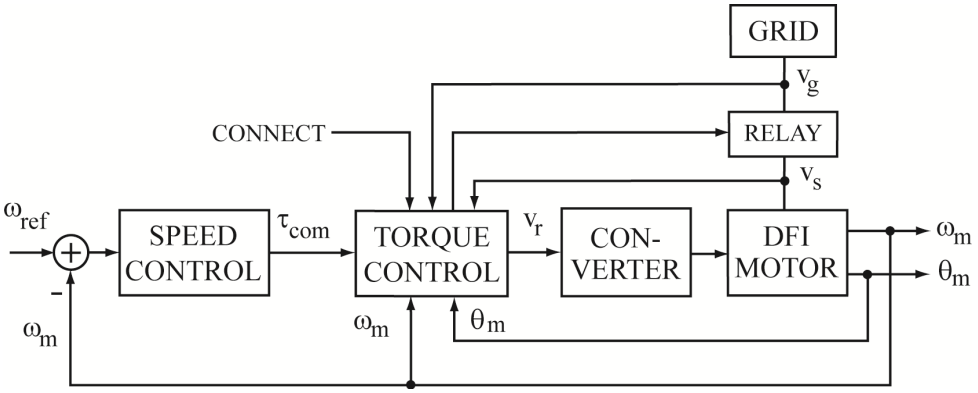

Fig. 4. Motor speed control algorithm

The torque control block serves both to synchronize the machine to the grid before connection and to control the torque of the motor when connected. The vector of rotor voltages $v_r = (v_{a,r}\ v_{b,r}\ v_{c,r})^T$ is computed using (7)-(9) to provide a torque equal to the command τ_{com} while absorbing a stator reactive power Q_{com} (not shown). The computation uses measurements of the rotor position θ_m, the rotor velocity ω_m, and the stator voltage vector $v_s = (v_{a,s}\ v_{b,s}\ v_{c,s})^T$. The actual stator frequency was estimated from the stator voltages using a frequency estimation algorithm derived from ref. [21].

Before connection to the grid, the grid voltage vector $v_g = (v_{a,g}\ v_{b,g}\ v_{c,g})^T$ is measured together with v_s , and the rotor voltage vector is computed to ensure that $v_s = v_g$. This situation corresponds to a zero torque and zero reactive power, implying zero stator currents. Therefore, a connection to the grid with zero transients is possible. When the voltages are equal, the operator engages the *connect* variable, which closes the relay between the grid and the DFI motor. The connection can also be performed automatically. Tuning parameters were inserted in the rotor voltage magnitude and phase to compensate for small discrepancies between the system and its model, as well as to remove the need to initialize the encoder providing the rotor position measurement.

On Fig. 4, the inner torque control algorithm is augmented by an outer loop for speed control that ensures the tracking of a reference command ω_{ref} by the speed ω_m. The speed control algorithm is a conventional proportional-integral control system with anti-windup protection. The torque command is limited to ensure that the predicted rotor currents stay within their limits. A proportional-integral control loop was also added using the variable Q_{com} to regulate the reactive power Q_s to zero.

Reactive power is a variable defined to quantify the fact that currents are larger than the minimum currents needed to transmit the power at the given voltages. The power factor is given by $PF = P_s/|P_s + jQ_s|$, so that PF=0.9 means that the real power P_s is 90% of the maximum power that could be exchanged with the same voltages and currents. Reactive power is not real and is not dissipated as heat. However, if power is transmitted over some distance (e.g., if the generator was in the tail of the plane and the motors under the wings), the excess currents would create real power losses in the wires that would be dissipated as heat. Voltage drops would also occur that would result in higher rotor currents and higher losses in the machines. For this reason, the controller was designed to achieve a unity power factor, or zero reactive power transfer.

C. DFIG Control

Most control methods proposed recently for DFIGs concern doubly-fed induction generators connected to the so-called infinite grid (as opposed to the stand-alone, local grid of this paper) [12]. A stand-alone application is considered in ref. [23] using dq control. Ref. [24] proposes a control system for a stand-alone DFIG, but with a DC load. This paper applies a control strategy similar to ref. [25] except that, as for the motor control, inner control loops are not used for the currents. Also, the control strategy for the DFIG is developed based on the steady-state model around the nominal condition I_s=0 and ω_r=0, so that

$$\frac{V_s}{V_r} = \frac{j\omega_s M}{R_r}. \tag{13}$$

In other words, the magnitude of the phasor V_s is proportional to the magnitude of the phasor V_r and its angle is equal to the angle for the rotor plus 90 degrees.

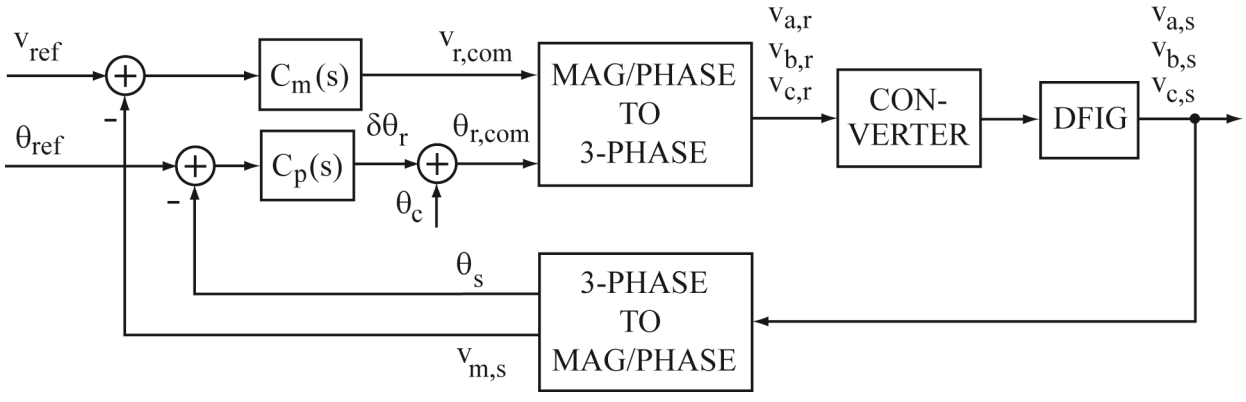

Fig. 5: Generator voltage control algorithm

Fig. 5 shows the diagram of a generator control algorithm based on this property. In the figure, v_{ref} is the reference value for the peak grid voltage (or stator voltage of the generator), while θ_{ref} is obtained by integration of the angular frequency ω_s. ω_s is set equal to the reference value $2\pi f_{ref}$,where f_{ref} is the reference value for the frequency of the grid (in Hz). The reference values are compared to the values obtained from measurements of the 3-phase stator voltages and applied to compensators for the magnitude, $C_m(s)$, and for the phase, $C_p(s)$. Both compensators were chosen to be pure integral compensators. Integral action is included in the magnitude path to ensure tracking of the voltage reference. In the phase path, it is also used to avoid having to initialize an incremental encoder. The rotor angle was computed using the feedforward correction term $\theta_c = \theta_{ref} - n_p\theta_m + \frac{\pi}{2}$ originating from the phasor definitions and (13). The reference value for the voltage v_{ref} was made proportional to ω_{ref}, resulting in a constant V/Hz property, much like variable-speed-drives for induction machines. Although multiple motors are linked to the same grid, the control strategy adopted here is such that the DFIG maintains the grid voltage and frequency while three DFI motors are independently speed-regulated by their own inverter and controller pairs.

III. Hardware Verification

A. Experimental Test Bed

To verify the general operation of the fully DFIM-based AC system, a Low Power Test Bed (LPTB) was implemented. In this test bed, a DFIG replaces the stiff AC source of the system described in ref. [11]. The system is shown schematically in Fig. 6 and a photograph is shown in Fig. 7.

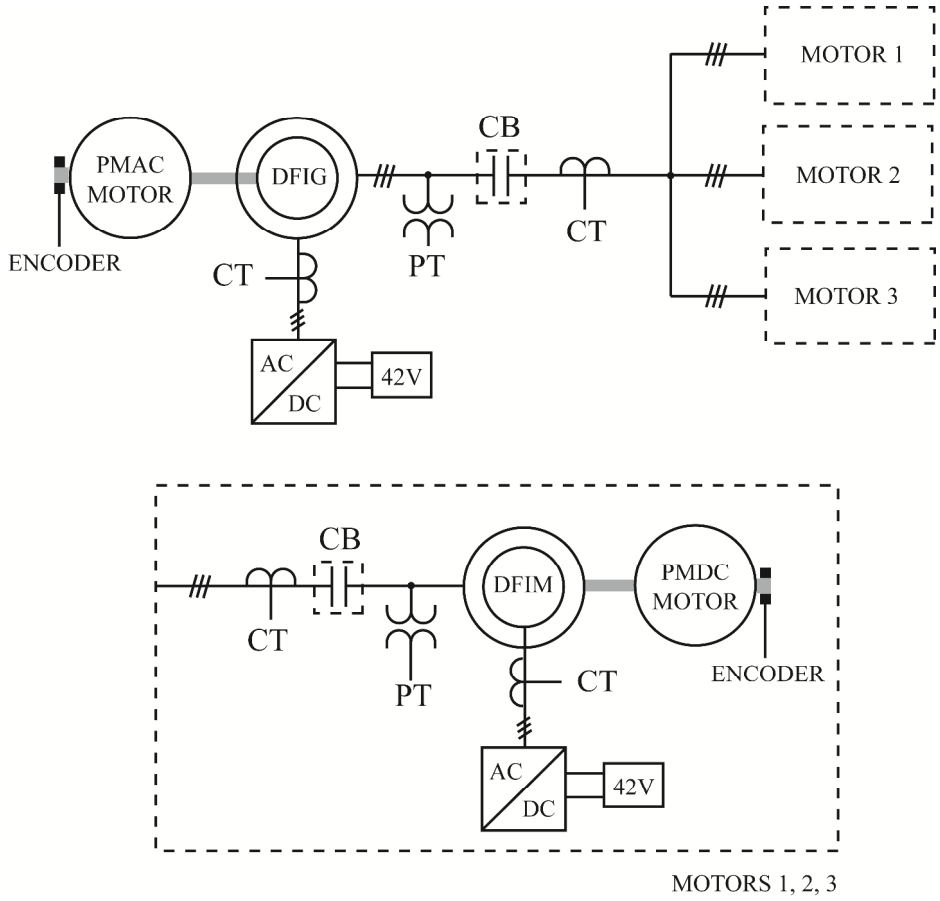

Fig. 6: Low Power Test Bed schematic (top: overall scheme, bottom: close-up for each motor)

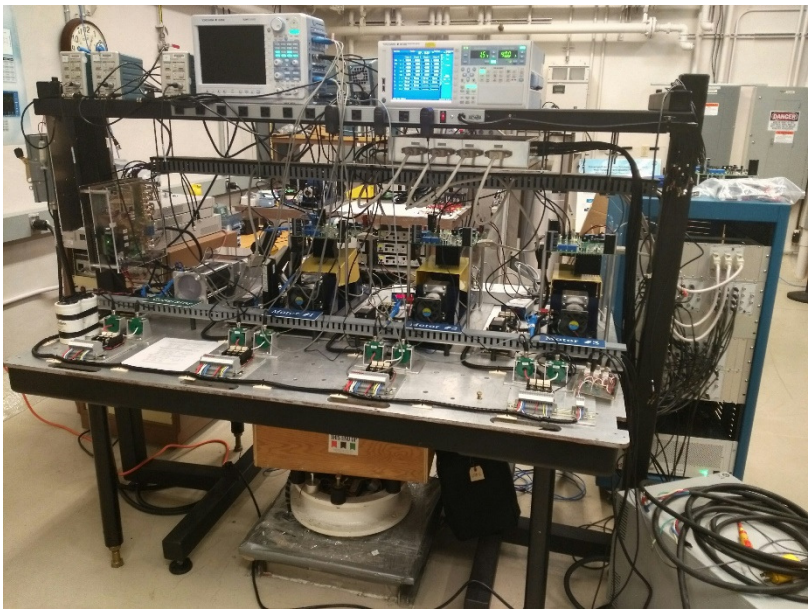

Fig. 7: Picture of the Low Power Test Bed

The top of Fig. 6 shows one DFIG and three DFIMs used as motors. The bottom of Fig. 6 shows the detail of the sub-systems associated with each motor. The machines have 2 pole pairs and are rated for 120 Hz operation, resulting in a synchronous speed of 3600 rpm. The rated stator voltage was 30 Vrms line-line, but was reduced to 24 Vrms at 120 Hz due to limitations of the generator. The rated power of the generator was 750W and the rated power of each motor was 250 W. The electrical machines are all manufactured by *Motorsolver*.

Fig. 6 shows contactors/breakers (CB) that were used to connect and disconnect the motors. A permanent-magnet AC motor with a variable speed drive was used as prime mover for the generator. The motors were connected to permanent-magnet DC motors that had encoders mounted on them to provide velocity information. The DFIMs were controlled by three-phase inverters from *Vishay* and connected to a 42V DC supply.

The instrumentation included voltage probes, labelled PT (for potential transducer) and current probes, labelled CT (for current transducer). Two systems were used for data collection: a Yokogawa ScopeCorder model DL850E and a data acquisition and control system with analog/digital converters and encoder interfaces from *dSPACE*. The control code ran at a sampling frequency of 2.5 kHz on the dSPACE system. Voltage and current measurements were filtered by first-order analog filters with 2.64 kHz bandwidth.

Accuracy of measurements: voltages and currents were digitized with 12 bit accuracy, providing a resolution of 0.0667 V and 0.0167 A, respectively. Manufacturer data specified a ±0.5% accuracy at full range, resulting in estimated accuracies of ±0.5 V and ±0.125 A, respectively. The encoders provided position data with resolution of 0.09 deg. The accuracy of the speed measurement with sampling at 2.5 kHz was deduced to be ±37 rpm. To improve steady-state accuracy, the velocity estimate was averaged over multiple samples, effectively increasing the sampling period and resulting in an estimated accuracy of about ±0.06 rpm.

B. Overview of Tests Performed

To verify the operation of the system and its components, multiple tests were performed and demonstrated on the test bed. These tests include: the ability of the motors to independently synchronize to the generator, the smooth startup of the motors to nominal speed, the differential speed control of the motors, tracking of a flight profile, the ability of the motors to maintain a constant speed despite generator speed changes, andthe ability of the generator to shift frequency while maintaining constant motor speeds. The controller parameters were set based on estimates of the machine parameters and adjusted manually during initial experiments with a single motor. Then, the same code was copied three times to control the three separate motors as described in the following sections.

C. Synchronization

The ability of the DFI motors to synchronize to the grid is demonstrated in Figs. 8 and 9 with the Motor 2 synchronization taken as an example. To synchronize the motor to the generator voltages (or local grid), the rotor voltage is computed using (13). Small adjustments of the rotor voltage magnitude and phase are applied so that the stator voltages match the grid voltages. Once the waveforms match closely, the contactors are closed, locking the stators of the machines and enabling closed-loop speed control. In the test bed demonstration, this process was performed manually with a scope and was significantly easier than for a synchronous generator, because the waveforms were stationary despite the speeds of the generator and motor not being matched.

In Fig. 8, as in all subsequent plots, the voltages shown are the line-line voltages $v_{ab,s}= v_{a,s-} v_{b,s}$ for the stator, and similarly for the grid. The stator current shown is the line current $i_{a,s}$, and similarly for the rotor current. As one can see in Fig. 8, before the synchronizing contactor is closed at approximately 4.093 seconds, the stator voltage of motor 2 is aligned with the grid voltage. There is no stator current present during this time as the stator of the motor is open circuit. After the voltages are synchronized, the contactor is closed and the motor is tied to the grid. A small stator current appears after the closing of the contactor, but this small current is mostly reactive (shared magnetizing current between the rotor and stator circuits). Over this process, the rotor of motor 2 stays still at zero RPM, as shown in Fig. 9.

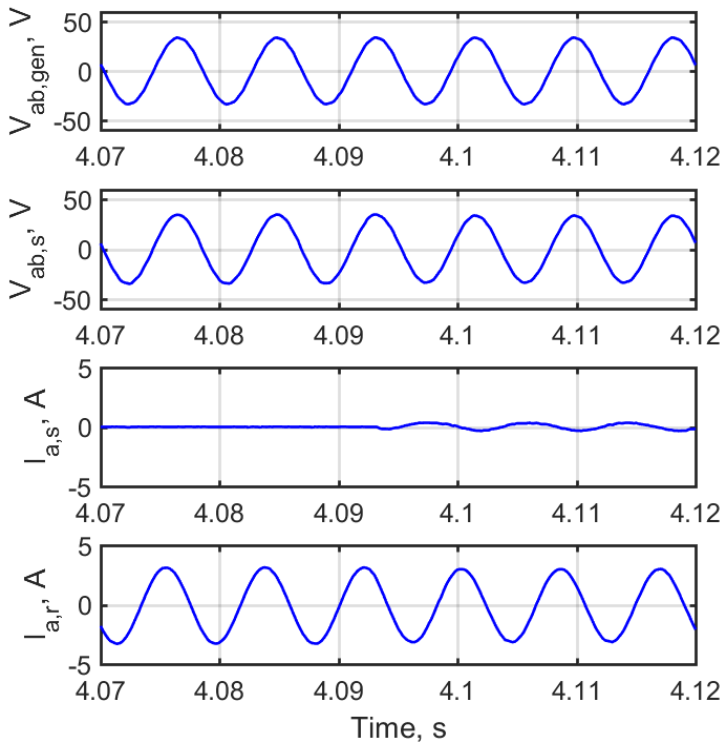

Fig. 8: From top to bottom: grid line-line voltage, motor 2 stator line-line voltage, motor 2 stator line current, motor 2 rotor line current (synchronization test)

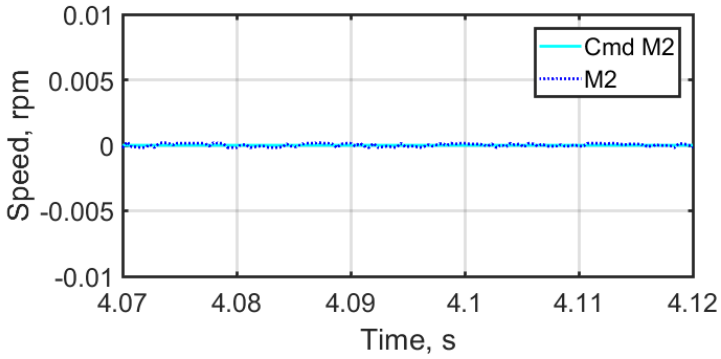

Fig. 9: Motor 2 speed (M2) and motor 2 command (Cmd M2) (synchronization test)

D. Startup

The speed responses of the three motors commanded from standstill to synchronous speed at 3600 RPM are shown in Fig. 10, along with their power factor. The active and reactive powers absorbed by the stators were estimated using

(4) and instantaneous estimates of the phasors obtained from a 3-phase to 2-phase transformation. For plotting, the instantaneous power factor was filtered by a first-order filter with pole at 0.5 rad/s.

The grid voltage and stator/rotor current data for Motor 2 are shown in Fig. 11. The generator was running at a nominal speed of 3600 RPM and set to provide 24 Vrms line-line at 120 Hz. As one can see, the motors track the startup command accurately, in addition to maintaining very close to unity power factor (which corresponds to zero reactive power). The starting currents of the motors stay within acceptable values. For a full-scale system, limiting of the currents may be desirable, and could be based on the more advanced version of the algorithm [22]. A slower rise of the currents could also be obtained by filtering the speed reference in order to prevent excitation of flexible modes.

Concerning the generator controller, there is a small dip in the grid voltage during the initial start. This voltage drop on the grid could be mitigated by staggering the motor commands with a slight time delay or by coordinating the control systems of the generator and the motors.

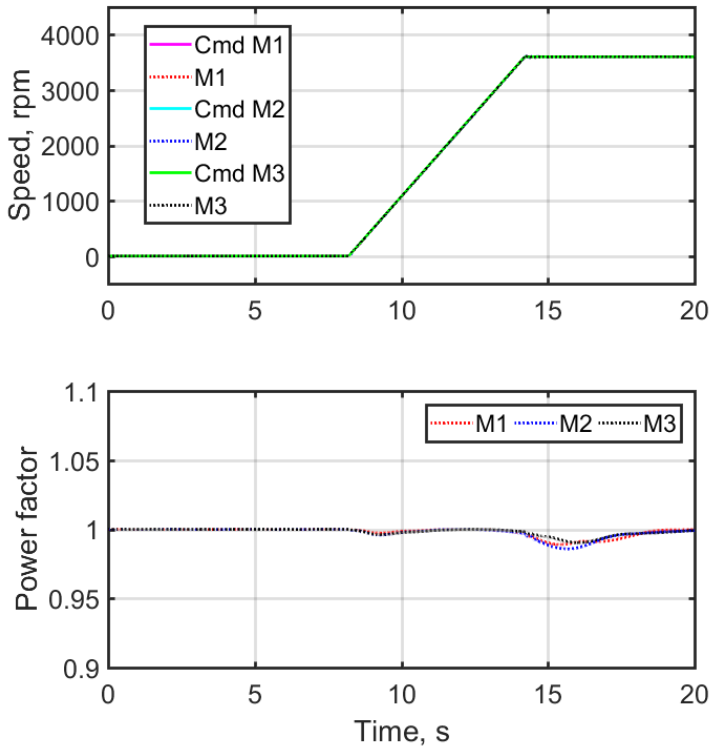

Fig. 10: From top to bottom: motor speeds and commands, motor power factors (startup test). Note that the speed responses are in close agreement and overlap with each other.

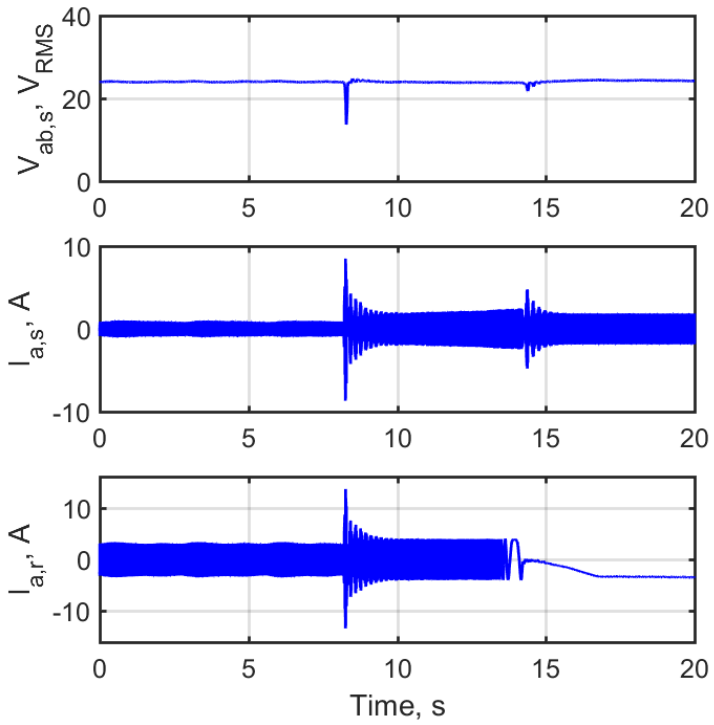

Fig. 11: From top to bottom: grid line-line voltage (rms value), motor 2 stator line current, motor 2 rotor line current (startup test)

E. Differential Operation

The capability of the three parallel motors to operate differentially and concurrently is shown in Figs. 12 and 13. The generator is again running at a nominal speed of 3600 RPM and set to provide 24 Vrms line-line at 120 Hz. The motors track their respective speed commands accurately during the test and at close to unity power factor. Considering the generator, the grid voltage stays at its nominal value except for a small dip when all the motors accelerate together. Differential operation of the motors could be used to generate a yaw moment using the propulsion system. Although the rotor current observed in Fig. 13 is much smaller around t=100 s than around t=25 s, the full

data shows that the overall current magnitude is about the same, but flows from phase b to phase c instead of phase a to phase b.

/

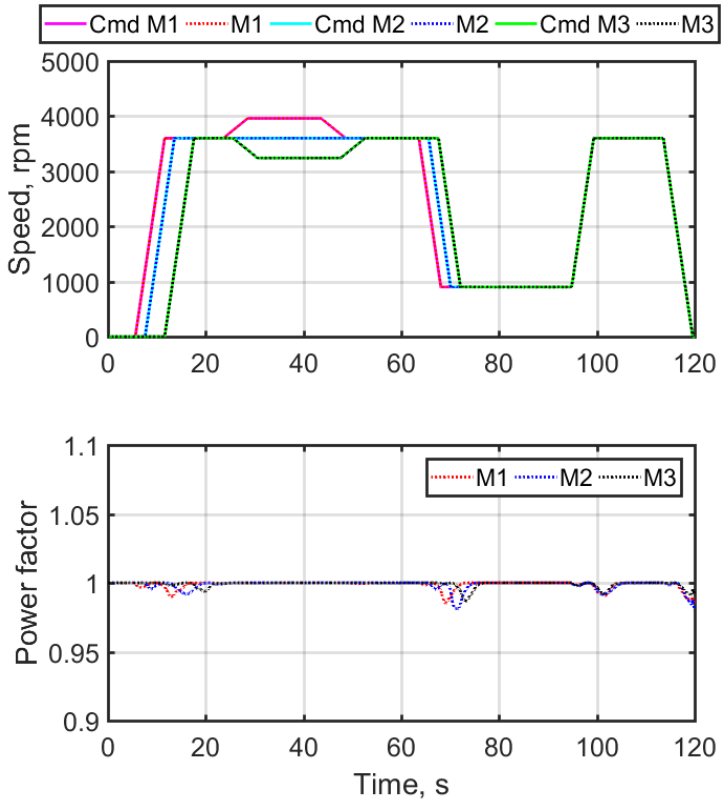

Fig. 12: From top to bottom: speeds of motors 1, 2, and 3 (M1, M2, M3) and respective commands (Cmd M1, Cmd M2, Cmd M3), motor power factors (differential test). Note that the speed responses and references are in close agreement and overlap with each other.

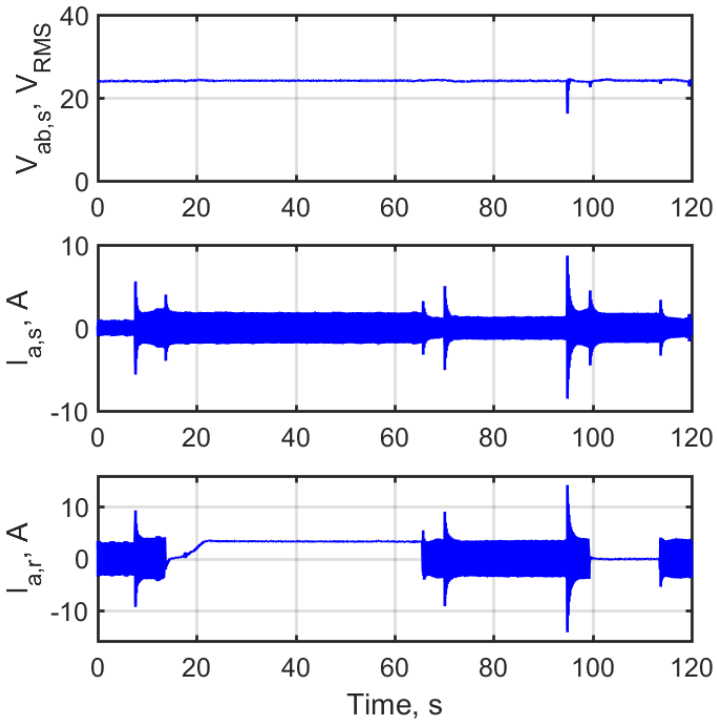

Fig. 13: From top to bottom: grid line-line voltage (rms), motor 2 stator line current, motor 2 rotor line current (differential test)

F. Flight Profile Tracking

The ability of the propulsors to follow commands corresponding to a flight profile is investigated using a hypothetical profile shown in Fig. 14. The high thrust on landing is associated with conventional thrust reversers. With electric propulsion, the speed of rotation could also be reversed. Preferably, pitch control of the fans could be used, if available. The results are shown in Fig. 15 using a generator voltage of 24 Vrms line-line at 120 Hz. The motors track the speed profile with no visible deviation from the setpoints and with near unity power factor. The Motor 2 voltage and current data is plotted in Fig. 16. There is a small voltage dip only at the start of the profile, which could be mitigated as described earlier.

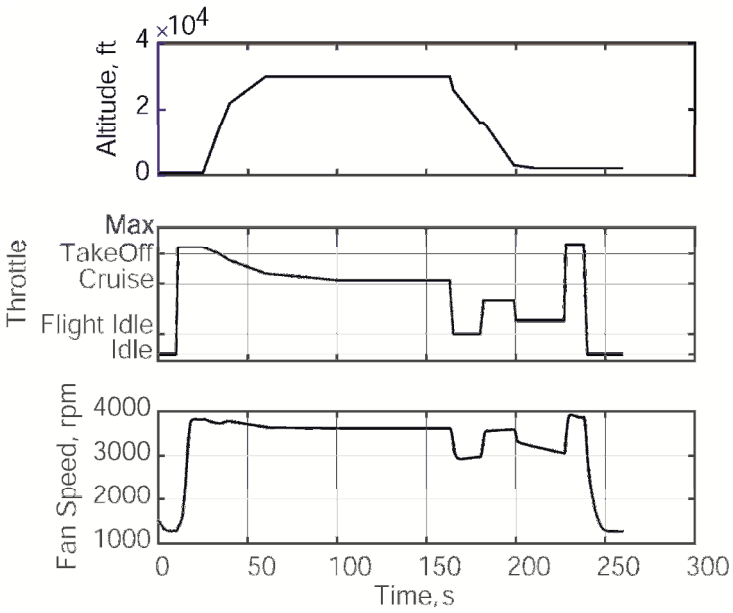

Fig. 14: Hypothetical flight profile

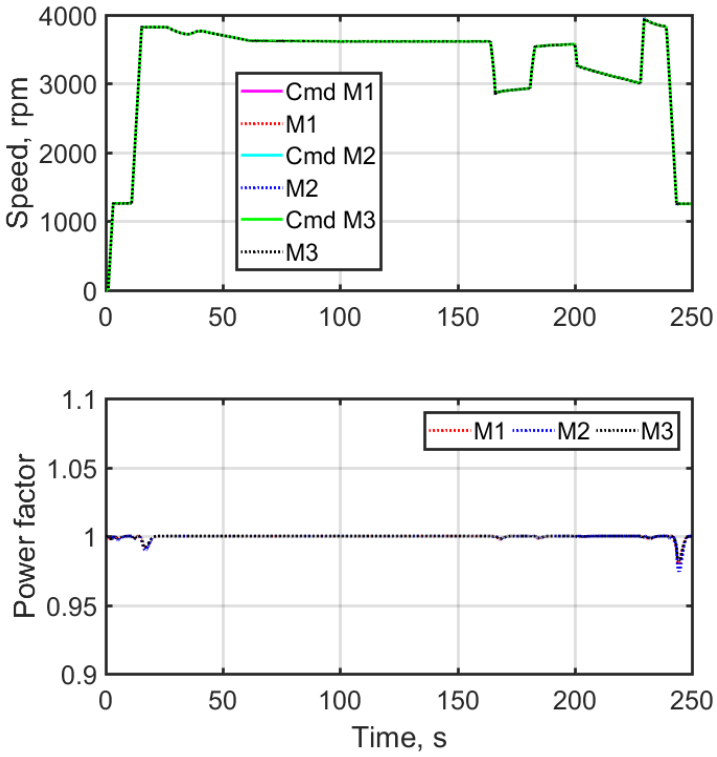

Fig. 15: From top to bottom: speeds of motors 1, 2, and 3 (M1, M2, M3) and respective commands (Cmd M1, Cmd M2, Cmd M3), motor power factors (flight profile test). Note that the speed responses are in close agreement and overlap with each other.

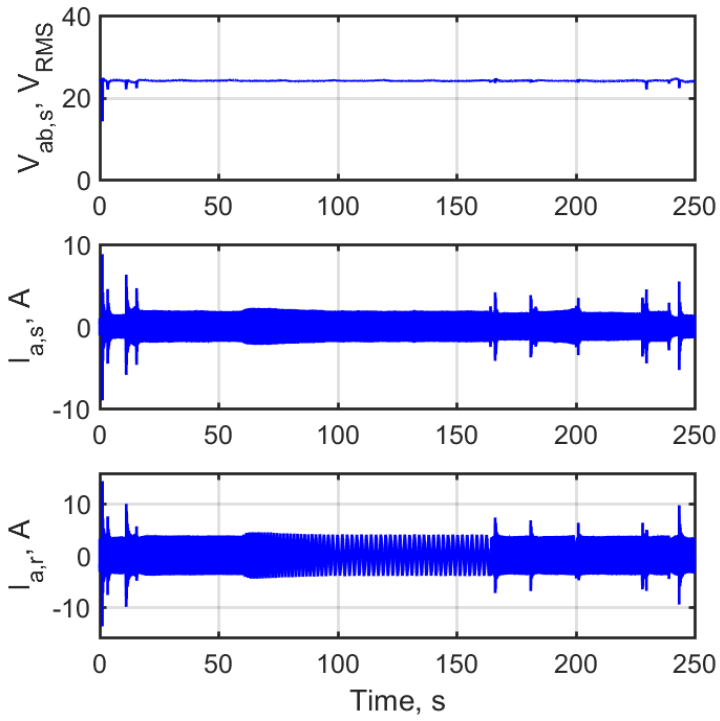

Fig. 16: From top to bottom: grid line-line voltage (rms), motor 2 stator line current, motor 2 rotor line current (flight profile test)

G. Generator and Motor Regulation with Varying Prime Mover Speed

The effect of varying the speed of the prime mover (turbine) is explored by starting the generator at 3150 RPM, and adjusting its speed ± 15% around the nominal speed, as shown in Fig. 17. It should be noted that the drive motor had a rate limit so that the acceleration was limited by the hardware. The generator voltages, set to 21 Vrms line-line at 105 Hz for the initial 3150 RPM speed, kept their frequency and the motors kept their speed despite significant variations in the turbine speed. The tracking becomes slightly oscillatory when the generator is driven at low speed. This oscillation being small was not immediately noticed and might be corrected by using a gain-scheduled controller tuned for multiple operating points.

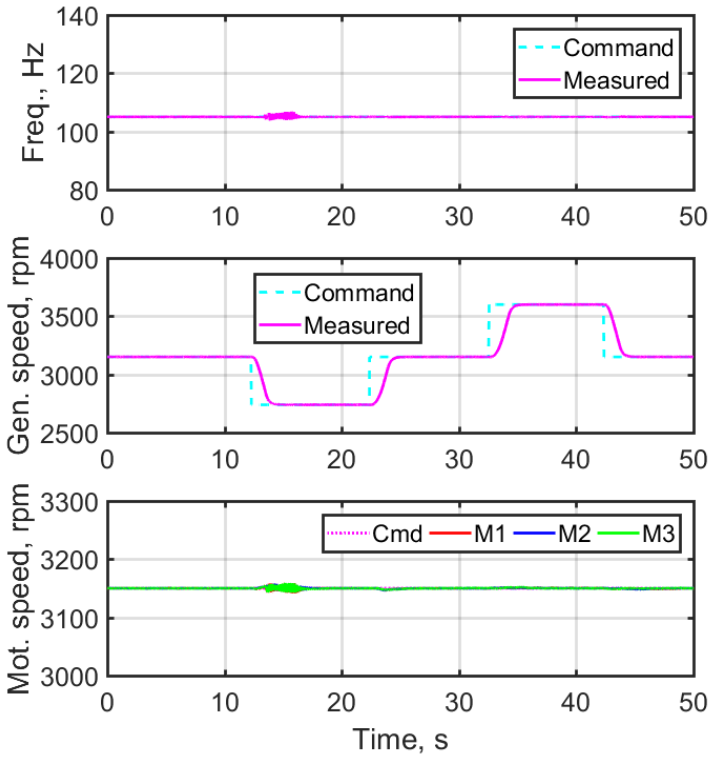

Fig. 17: From top to bottom: grid frequency, generator speed, and motor speeds (prime mover speed variation test)

H. Voltage and Frequency Control with Steady Prime Mover Speed

The generator was operated under load (parallel motors spinning at 3150 RPM) at initial settings of 3150 RPM and 21 Vrms line-line at 105 Hz. The voltage and frequency references were varied with steps of ± 15% about the nominal operating point as shown in Fig. 18. The tracking capability of the generator controller is shown to be both accurate and responsive as the motors maintain their desired setpoint values with little deviation.

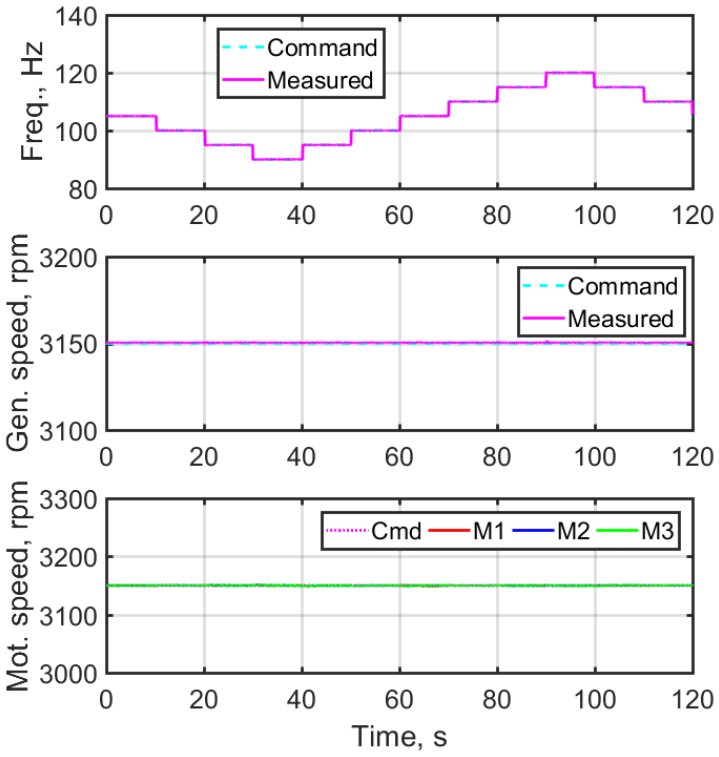

Fig. 18: From top to bottom: grid frequency, generator speed, and motor speeds (generator voltage and frequency variation test)

IV. Discussion of Electric Propulsion Options

The architecture studied in this paper constitutes a solution intermediate between the architecture of Fig. 1 showing full conversion from AC to DC and DC to AC, and the architecture of Fig. 19 showing direct AC connection between the generator and the motor (or motors). Fig. 19 assumes that a synchronous generator is fed by a DC/DC converter connected a DC bus. The DC bus is supplied by a storage element (battery or ultracapacitor) and by an AC/DC converter on the AC bus. The motor could be a permanent-magnet synchronous motor or a cage rotor induction motor.

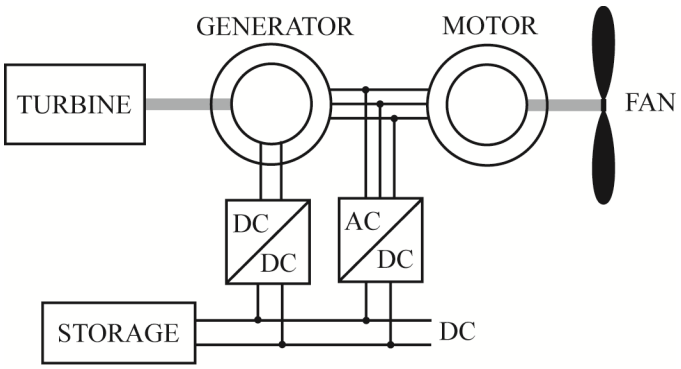

Fig. 19. AC power architecture without DFIMs

Advantages of the architecture of Fig. 19 are the direct transfer of power with minimal losses and the low ratings of the converters. The AC/DC converter could be a simple rectifier. A permanent-magnet synchronous motor would be highly efficient and compact, but also problematic. If a disturbance caused loss of synchronism, the speed of the motor would collapse, and the speed of the generator would need to be brought down to restart the motor. If multiple motors were connected in parallel, the stalled motor would need to be disconnected, or the speed of all the motors would need to be brought down to restart the system.

With the DFIM architecture of Fig. 2, the rotor-side converters provide a high level of controllability of the machines, considerably increasing the stability of the system. In fact, an improvement of Fig. 19 would be the replacement of the synchronous generator by a DFIG. Using the capability for multiple motors in parallel, however, would be non-trivial.

If a cage rotor induction motor is used in Fig. 19, the speed of the motor would be a few percent smaller than the synchronous speed, which is equal to the speed of the generator multiplied by the ratio of the number of pole pairs of the generator and of the motor. Cage rotor induction motors are inherently much more stable than synchronous motors. However, there is still no capability of adjustment of the speed of the motor, which is tied to the generator speed. Efficiency is also lower, because the induction motor always operates sub-synchronously and all the energy converted on the rotor side is lost in heat.

In contrast, the DFIM architecture of Fig. 2 gives the ability to modulate the speed of the motor and to regenerate the power drawn from the rotor. Higher efficiencies may be attained by using the synchronous and super-synchronous modes of the DFIMs. A boost of power may also be drawn from storage with proper energy management. In addition, the turbine is allowed to operate at a more constant speed and with better efficiency.

At the opposite end of the spectrum, the architecture of Fig. 1 with full DC/DC converters also solves the problems of Fig. 19, with greater flexibility than the DFIM architecture of Fig. 2. The speeds of the turbine and of the motor can be made completely independent, and the flow of energy between the turbine, motors, and storage is simpler to manage. However, DFIMs could be operated with smaller-size converters, resulting in lower weight and lower conversion losses. Lower conversion losses would result in lower weight of the cooling systems as well. Overall, the benefits could well justify the use of the DFIM architecture.

Another consideration is the fault tolerant capability of the architecture. In the DC solution of Fig. 1, options are very limited if *either* converter fails. In the DFIM architecture, the generator could be operated synchronously if one of three legs of its converter failed. The DFI motors could be operated synchronously in a similar situation, or as conventional induction motors if the motor converter failed. Indeed, a DFIM with a short-circuited rotor is equivalent to a cage rotor induction motor. Operation would be degraded, but various options could be exploited to sustain flight until repairs can be made.

V. Future research

The control system proposed in the paper is only a small component of what would be a broader system including turbine control, pitch control of fans, and energy storage control. A major topic of future research is the integration of this inner-loop control system within a higher-level energy management system. Such system would manage the energy flow between the turbine, the generator, the motor(s), and the energy storage. The speed of the turbine, the voltage of the grid, and the frequency of the grid are control variables that determine how power flows through the machines and how much energy is sent to or retrieved from storage. A strategy would need to be developed to coordinate these variables to optimize efficiency while respecting the constraints of the system.

Experiments at progressively higher power levels would be beneficial, as well as a detailed simulation of a system at the full scale. The evaluation could include additional factors not considered in this paper, such as variable fan loading in turbulent environments, contribution of electric propulsion to maneuvering, protection of the systems, and degraded modes of operation after failures. Technological issues need to be resolved regarding the design of the systems and the organization of the components in the airframe. Current and future topics of research include the design of high voltage/high speed machines, construction of machines and converters for high efficiency and high power density, multi-phase machines, and high-density storage components.

VI. Conclusions

The control, integration, and testing of a fully DFIM-based system is described with a potential application to hybrid electric propulsion of aircraft. The system is shown to operate in a quick, responsive, and stable manner for multiple tests. Only minor issues were encountered, including a grid voltage dip when all the motors were started at the same time. Such transients could be mitigated by staggering the motor speed commands or by coordinating the motor and generator controllers. The experiments demonstrated the ability to separate the mechanical speed from the electrical frequency. As a result, motor and generator speeds were decoupled. Another benefit is the reduced size of the power converter needed for the motors and generator. This benefit requires some coordination between the voltage, frequency, and speed control, a subject of further research.

Some of the benefits demonstrated in this paper could be achieved with combinations of different machines, such as a synchronous generator driving multiple DFI motors or a DFIG driving multiple cage rotor induction machines, or even permanent-magnet synchronous machines. Multiple generators could also be connected in parallel using some coordinated control method. Future work is expected to occur using a higher power test bed, which should lend itself to offering data at voltage, frequency, and current levels closer to what a future hybrid electric aircraft might use.

VII. Acknowledgments

The authors would like to acknowledge funding from NASA's *Convergent Aeronautics Solutions High Voltage-Hybrid Electric Propulsion* task and thank Ray Beach in support of this effort, along with Jim Dolce, Tom Balogas, David Hausser, and George Horning for their assistance in the construction of the low power test bed. Ray Beach is particularly thanked for his leadership and vision. The first author is thankful for the support received from the *Advanced Research and Technology Support* (ARTS) subcontract 04555-024 (task order number 0455.13TA87T.06.00.U10) through the *Universities Space Research Association* (USRA) and *NASA Glenn Research Center*. The other authors are employees of the U.S government's *National Aeronautics and Space Administration* that directly funded their research. In addition, the authors thank the reviewers and the associate editor for many constructive comments, which contributed significantly to the revised version of this paper.

VIII. References

[1] Sarlioglu, B., & Morris, C.T., "More Electric Aircraft: Review, Challenges, and Opportunities for Commercial Transport Aircraft," *IEEE Transactions on Transportation Electrification*, vol. 1, no. 1, 2015, pp. 54-64.

doi:10.1109/TTE.2015.2426499

[2] Pornet, C., & Isikveren, A.T., "Conceptual Design of Hybrid-Electric Transport Aircraft," *Progress in Aerospace Sciences*, vol. 79, 2015, pp. 114–135.

doi: 10.1016/j.paerosci.2015.09.002

[3] Smith, H., "Airframe Integration for an LH2 Hybrid-Electric Propulsion System," *Aircraft Engineering and Aerospace Technology*, vol. 86, no. 6, 2014, pp. 562-567.

doi: 10.1108/AEAT -04-2014-0045

[4] Gohardani, A.S., Doulgeris, G., & Singh, R., "Challenges of Future Aircraft Propulsion: A Review of Distributed Propulsion Technology and its Potential Application for the All Electric Commercial Aircraft," *Progress in Aerospace Sciences*, vol. 47, 2011, pp. 369–391. doi:10.1016/j.paerosci.2010.09.001

[5] Reynolds, K., Nguyen, N., Ting, E., & Urnes, J., "Wing Shaping Concepts Using Distributed Propulsion," *Aircraft Engineering and Aerospace Technology*, vol. 86, no. 6, 2014, pp. 478–482.

doi:10.1108/AEAT-04-2014-0050

[6] Glassock, R., Galea, M., Williams, W., & Glesk, T., "Hybrid Electric Aircraft Propulsion Case Study for Skydiving Mission," *Aerospace*, vol. 4, no. 45, 2017, pp. 1-22.

doi:10.3390/aerospace4030045

[7] Friedrich, C., & Robertson, P.A., "Hybrid-Electric Propulsion for Aircraft," *Journal of Aircraft*, vol. 52, no. 1, 2014, pp. 176-189.

doi:10.2514/1.C032660

[8] Hung, J. Y.-C., & Gonzalez, L.F., "On Parallel Hybrid-Electric Propulsion System for Unmanned Aerial Vehicles," *Progress in Aerospace Sciences*, vol. 51, 2012, pp. 1-17.

doi:10.1016/j.paerosci.2011.12.001

[9] Schiltgen, B., Green, M., Freeman, J., & Gibson, A., "Terminal Area Operations for Hybrid Electric Distributed Propulsion," *Aircraft Engineering and Aerospace Technology*, vol. 86, no. 6, 2014, pp. 584-590.

doi:10.1108/AEAT-04-2014-00472

[10] Sadey, D.J., Taylor, L.M., & Beach, R.F., "Proposal and Development of a High Voltage Variable Frequency Alternating Current Power System for Hybrid Electric Aircraft", *14th International Energy Conversion Engineering Conference*, AIAA 2016-4928, Salt Lake City, UT, July 25-27, 2016.

doi:10.2514/6.2016-4928

[11] Sadey, D.J., Bodson, M., Csank, J., Hunker, K., Theman, C., & Taylor. L., "Control Demonstration of Multiple Doubly-Fed Induction Motors for Hybrid Electric Propulsion," *53rd AIAA/SAE/ASEE Joint Propulsion Conference*, *AIAA Propulsion and Energy Forum*, AIAA 2017-4954, Atlanta, GA, July 10-12, 2017.

doi:10.2514/6.2017-4954

[12] Muller, S., Deicke, M., & De Doncker, R.W., "Doubly Fed Induction Generator Systems for Wind Turbines," *IEEE Industry Applications Magazine*, vol. 8, no. 3, 2002, pp. 26-33.

doi:10.1109/2943.999610

[13] Yuan, X., Chai, J., & Li, Y., "A Converter-Based Starting Method and Speed Control of Doubly Fed Induction Machine With Centrifugal Loads," *IEEE Transactions on Industry Applications*, vol. 47, no. 3, pp. 1409-1418, 2011.

doi:10.1109/TIA.2011.2125937

[14] Zhang, Y., & Ooi, B. T., "Adapting DFIGs for Doubly-Fed Induction Motors Operation," *2012 IEEE Power and Energy Society General Meeting*, San Diego, CA, 2012, pp 1-8.

doi:10.1109/PESGM.2012.6345113

[15] Banerjee, A., Tomovich, M. S., Leeb, S. B., & Kirtley, J. L., "Control Architecture for a Switched Doubly Fed Machine Propulsion Drive," *IEEE Transactions on Industry Applications*, vol. 51, no. 2, pp. 1538-1550, 2015.

doi:10.1109/TIA.2014.2347452

[16] Abdellatiff, M., Debbou, M., Slama-Belkhodja, I., & Pietrzak-David, M., "Simple Low-Speed Sensorless Dual DTC for Double Fed Induction Machine Drive," *IEEE Transactions on Industrial Electronics*, vol. 61, no. 8, pp. 3915-3922, 2014.

doi:10.1109/TIE.2013.2288190.

[17] Poddar, G., & Ranganathan, V.T., "Direct Torque and Frequency Control of Double-Inverter-Fed Slip-Ring Induction Motor Drive," *IEEE Transactions on Industrial Electronics*, vol. 51, no. 6, 2004, pp. 1329-1337.

doi: 10.1109/TIE.2004.837897

[18] Liu, Y., & Xu,,L., "The Dual-Current-Loop Controlled Doubly Fed Induction Motor for EV/HEV Applications," *IEEE Transactions on Energy Conversion*, vol. 28, no. 4, 2013, pp. 1045-1052.

doi: 10.1109/TEC.2013.2279853

[19] Bonnet, F., Vidal, P.-E., & Pietrzak-David, M., "Dual Direct Torque Control of Doubly Fed Induction Machine," *IEEE Transactions on Industrial Electronics*, vol. 54, no. 5, 2007, pp. 2482-2490.

doi: 10.1109/TIE.2007.900330

[20] Mohammed, O.A., Liu, Z., & Liu, S., "A Novel Sensorless Control Strategy of Doubly Fed Induction Motor and Its Examination with the Physical Modeling of Machines," *IEEE Transactions on Magnetics*, vol. 41, no. 5, 2005, pp. 1852-1855.

doi:10.1109/TMAG.2005.846500

[21] Pigg, S., & Bodson, M., "A New Algorithm for Frequency Estimation and Disturbance Cancellation Inspired from Induction Machine Theory," *Proceedings of the American Control Conference*, San Francisco, CA, pp. 3018-3023, 2011.

doi:10.1109/ACC.2011.5991372

[22] Bodson, M., "Speed Control for Doubly Fed Induction Motors With and Without Current Feedback," to appear in *IEEE Transactions on Control Systems Technology* (available in early access on *ieeexplore*, 2019).

doi: 10.1109/TCST.2019.2898372

[23] Naidu, N.K.S., & Singh, B., "Experimental Implementation of Doubly Fed Induction Generator-Based Standalone Wind Energy Conversion System," *IEEE Transactions on Industry Applications*, vol. 52, no. 4, 2016, pp. 3332-3339.

doi: 10.1109/TIA.2016.2542783

[24] Misra, H., & Jain, A.K., "Mathematical Modeling and Control of Standalone DFIG-DC System in Rotor Flux Reference Frame," *IEEE Transactions on Industrial Electronics*, vol. 65, no. 5, 2018, pp. 3708-3719.

doi: 10.1109/TIE.2017.2762644

[25] Shukla, R. D., & Tripathi, R. K., "Speed-Sensorless Voltage & Frequency Control in Autonomous DFIG Based Wind Energy Systems," *2014 Australasian Universities Power Engineering Conference*, Perth, WA, 2014, pp. 1-6.

doi:10.1109/AUPEC.2014.6966609